Chapter 7

Deep Level Transient Spectroscopy: A Powerful Experimental Technique for Understanding the Physics and Engineering of Photo-Carrier Generation, Escape, Loss and Collection Processes in Photovoltaic Materials

Aurangzeb Khan and Yamaguchi Masafumi

Additional information is available at the end of the chapter

http://dx.doi.org/10.5772/59419

1. Introduction

Deep Level Transient Spectroscopy (DLTS) is an efficient and powerful method used for observing and characterizing deep level impurities in semiconductors. The method was initially introduced by D. V. Lang [1] in 1974. DLTS is a capacitance transient thermal scanning technique, operating in the high frequency (Megahertz) range. It uses the capacitance of a p-n junction or Schottky barrier as a probe to monitor the changes in charge state of a deep centre. The capacitance techniques [2-10] used before DLTS lacked either in sensitivity, speed, range of observable trap depths, or the spectroscopic nature, thus rendering the techniques inadequate for a complete characterization of a deep level. DLTS has the advantage over all the techniques used to-date in that it fulfils almost all the requirements for a quick and complete characterization of a deep centre. DLTS is a technique, which is sensitive enough, rapid and easy to analyze. It is able to distinguish between majority- and minority-carrier traps [2]. DLTS can also give the concentrations, energy and capture rates of both kinds of traps. It is spectroscopic in the sense that it can also resolve signals due to different traps. In the many variants of the basic DLTS technique the deep levels are filled with free carriers by electrical or optical methods. Subsequent thermal emission processes give rise to a capacitance transient. The transient is analyzed by signal processing while the temperature is varied at a constant rate. This results in a full spectroscopic analysis of the semiconductor band-gap.

For a complete understanding of DLTS we must have some basic knowledge of capacitance transients arising from the depletion region of a p-n junction. The use of capacitance transients for studying the properties of defect centers is well known [4-6]. These transients provide

information about an impurity level in the depletion region by observation of the capacitance transient originating from the return to thermal equilibrium after a perturbation is applied to the system. A brief description of the capacitance change due to the change in occupancy of the deep levels in the depletion region is given below.

2. p-n junction capacitance

When voltage across a p-n junction is changed, there is a corresponding change in the depletion region width. This change in width causes a change in the number of free charge carriers on both sides of the junction, resulting in a change in the capacitance. This change has two contributions; a) the contribution due to change in depletion width known as the junction capacitance and b) the contribution due to change in minority carrier concentration called the diffusion capacitance. Junction capacitance is dominant under reverse biased conditions while diffusion capacitance is dominant under forward biased conditions.

Consider a p-n junction with a deep level present having its energy as E_T. In steady state there is no net flow of charge carriers across the trap. Also the electron and hole densities within the depletion region are negligible. Thus from Shockley and Reed [11] and Hall [12] the relationship between the total density of deep sates N_T and density of filled traps is given by

$$e_p n_T = \left(e_n + e_p\right) N_T \tag{1}$$

where e_p is the hole emission rate, e_n is the electron emission rate, n_T is the density of filled traps, and N_T is the total density of deep sates.

or

$$n_T = \left(\frac{e_p}{e_n + e_p}\right) N_T \tag{2}$$

which gives the density of filled traps n_T under steady state conditions.

Now if the system is perturbed, this number changes and will thus cause the total charge in the depletion region to increase or decrease, leading to a corresponding change in the capacitance. This change is only due to deep levels.

For a simple analysis of the response of the diode and interpretation of results, the junction is assumed to be asymmetric. An asymmetric diode is one in which one side of the junction is much more heavily doped than the other, implying that the space charge region is almost exclusively on the low doped side as shown in Figure. 1(a). Here we will consider a p^+n diode with an electron emitting level. The depletion region is thus on the n-side. Figure 1 (b)

http://dx.doi.org/10.5772/59419

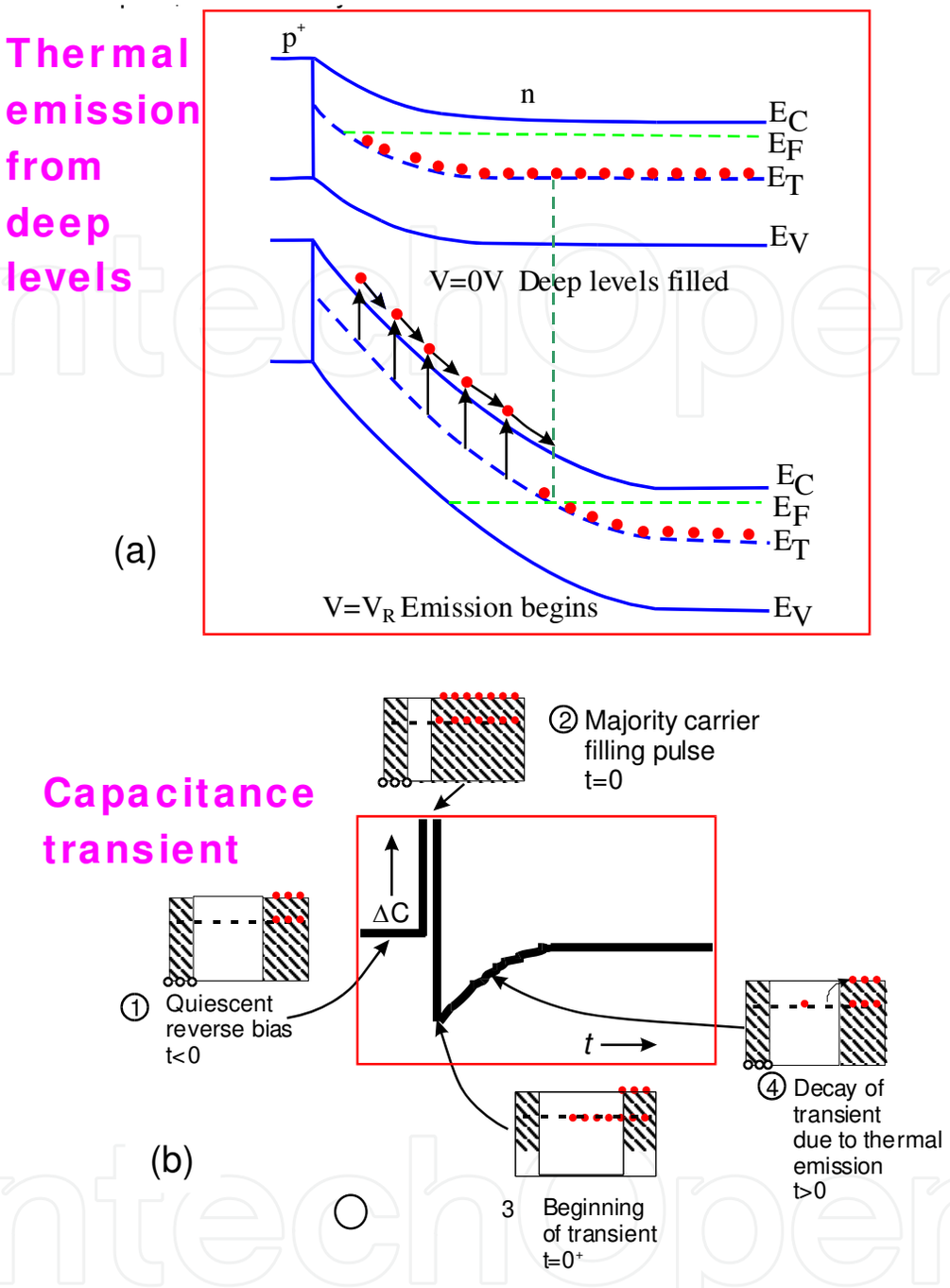

Figure 1. Basic concept of thermal emission from a deep level and capacitance transient (a) energy band diagram of a p^+n junction with an electron trap present at energy E_T at zero applied bias and at steady reverse bias V_R, (b) isothermal capacitance transient for thermal emission of the majority carrier traps. The condition for the trap occupation and free carrier concentration during various phases 1-4 of the transient are also shown. The part not shaded in the insets 1-4 shows space charge width (after Lang [1]).

schematically shows four processes of generating a capacitance transient due to majority carrier level.

Process (1) shows the diode in the quiescent reverse bias condition. Traps in the space charge region are empty because no free carriers are available for capture (t<0). Process (2): reverse

bias is reduced to zero by a majority carrier pulse. The electrons are capture in the deep levels (t=0). The sharp raise in capacitance is due to the collapse of the depletion region. Process (3): when the reverse bias is restored, the capacitance drops to a minimum value because the electrons are trap in the depletion layer ($t=0^+$). Process (4): decay of the transient due to thermal emission of the trapped electrons (t>0).

Suppose we have a reverse bias V_R applied to the sample and it is decreased for a short time to zero. Then electrons will flow into what was previously the depletion region and the levels in this volume will capture electrons (Figure. 1[a]). Neglecting the re-emission of electrons (i.e. temperature is low enough) we get:

$$\frac{dn_T}{dt} = c_n\left(N_T - n_T\right) \tag{3}$$

where c_n is the capture time constant of electrons

Now if bias pulse is long enough i.e. $t_p >> \frac{1}{c_n}$, all levels will be filled and $n_T = N_T$. Next the sample is returned to quiescent reverse bias V_R and thus the depletion region is again depleted of free carriers. The electron emitting traps now start to emit and n_T will vary with time. This variation is given by with n= p= 0 i.e.

$$\frac{dn_T}{dt} = e_p N_T - \left(e_n + e_p\right)n_T \tag{4}$$

The solution to this is given by

$$\begin{aligned} n_T(t) &= \left[\frac{e_p}{e_n + e_p}N_T + \frac{e_n}{e_n + e_p}N_T \exp\left(-\left(e_n + e_p\right)t\right)\right] \text{for } t > 0 \\ &= N_T \text{ for } t < 0 \end{aligned} \tag{5}$$

Thus n_T decreases exponentially with a time constant:

$$\tau = 1/\left(e_n + e_p\right) \tag{6}$$

Now for an electron emitting centre $e_n \gg e_p$. Equ. (5) then reduces to:

$$n_T(t) = N_T \exp\left(-e_n t\right) \tag{7}$$

Thus the amplitude of the transient describing the filled level population gives the measure of trap concentration, while the time constant gives the emission rate of electrons:

$$\tau = 1/e_n \tag{8}$$

The variation of occupancy with time gives information about the emission rate but it is not possible to measure the occupancy directly. The simplest indirect method is to measure the capacitance changes of the p-n junction associated with the occupancy changes.

The equation governing the capacitance of a p-n junction is the same as that of a parallel plate capacitor i.e.

$$C = \frac{\varepsilon A}{W} \tag{9}$$

where

$$W^2 = \frac{2\varepsilon\left(V_b - V\right)\left(N_D + N_A\right)}{qN_DN_A} \tag{10}$$

ε is the relative permittivity of the material, V_b is the built-in voltage, V is the applied voltage, q is the electronic charge, N_D and N_A are the donor and acceptor concentrations, W is the depletion region width and A is the junction area.

For a p^+n junction, including the contribution of the filled traps in the depletion region, this becomes:

$$W^2 = \frac{2\varepsilon\ \left(V_b - V\right)}{qN_D^*} \tag{11}$$

where $N_D^* = N_D - n_T$

Now for n_T « N_D one can expand and get the following result:

$$C = C_0\left(1 - \frac{n_T}{2N_D}\right) \tag{12}$$

where C_0 is the capacitance at reverse bias (V_R).

By taking into consideration the time variation of n_T, we get:

$$C(t) = C_0\left[1 - \frac{N_T}{2N_D}\exp\left(-\frac{t}{\tau}\right)\right] \tag{13}$$

Thus the emission rates and trap concentrations can be determined from the changes in the capacitance of a p-n junction due to bias pulses. These changes are in the form of capacitance transients.

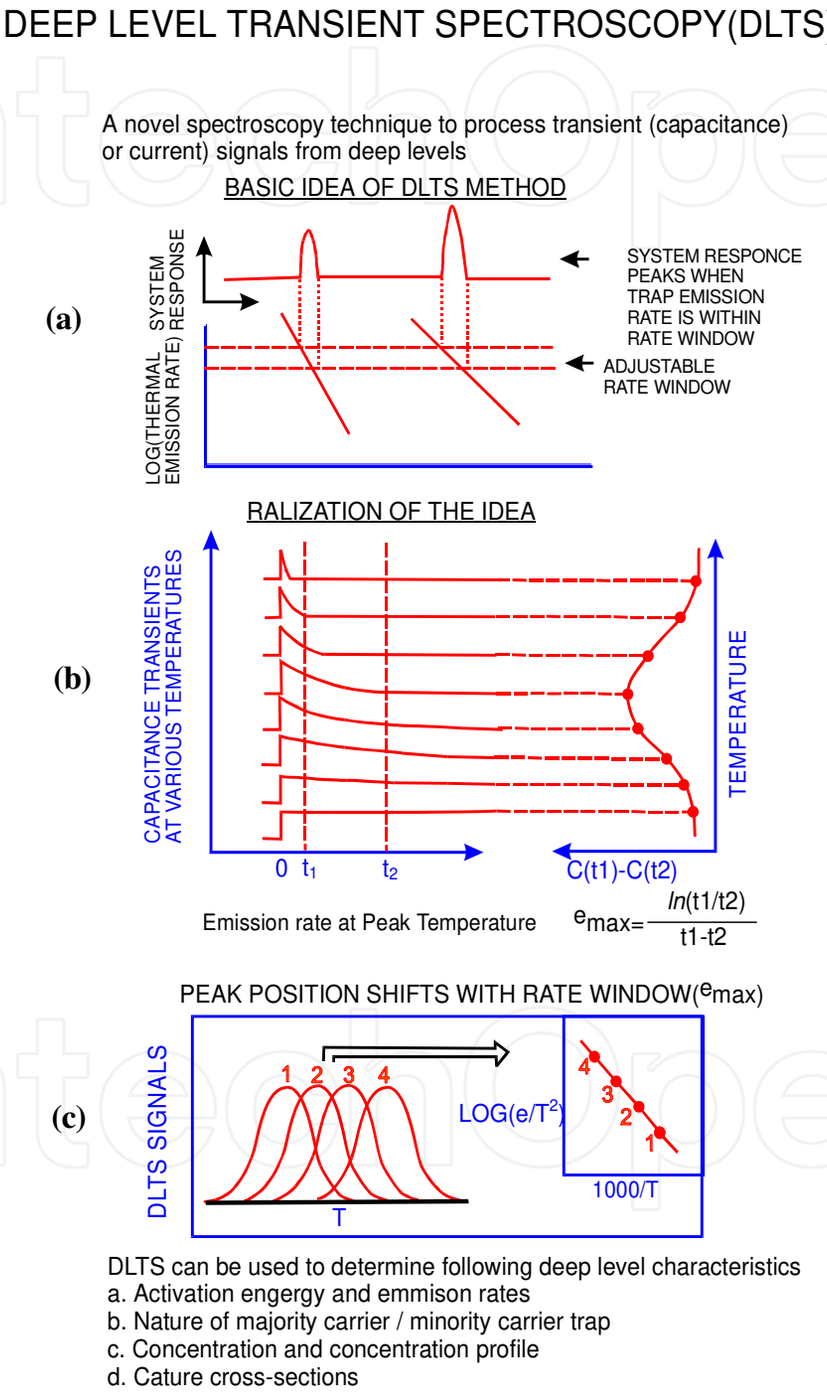

Figure 2. Diagram illustrating the basic principles of DLTS (a) the rate window concept (after Lange [1]), (b) application of the rate window concept using a time filter such as dual-gate box car shown here (after Lange [1]), (c) showing the shift of the peak positions in temperature with the rate window and the Arrhenius plot obtained from the peak positions ([31].

http://dx.doi.org/10.5772/59419

3. Basic methodology of DLTS

The capacitance transients of Eq. 13 can be obtained by holding the sample at constant bias and temperature and applying a single filling pulse. The resultant isothermal transient can then be analyzed to obtain the emission rate of the carriers at that particular temperature. For obtaining a wide range of emission rates, this is a time consuming technique. Also if a lot of deep levels are present, the experiment and its analysis become difficult. This is where DLTS has a major edge over the conventional techniques.

The essential feature of DLTS [1] is its ability to set up a *rate window* so that the measuring apparatus gives an output only when a transient occurs with a rate within the window. This concept is illustrated in Figure 2 (adopted with permission from IEEE Proc. of WCPEC-4, 2006, p. 1763).Thus if the sample temperature is varied at a constant rate, causing the emission rate of carriers from defect center(s) present in it to vary, the measuring instrument will give a response peak whenever the defect center emission rate is within the window. Instead of talking about rate window, we can say that the DLTS technique uses a time filter, which gives an output signal only when the transient has a time constant coinciding with the center of the time window of the filter. A very important property of such a filter (time or rate) is that the output is proportional to the amplitude of the transient. Thus we can excite the diode repeatedly while the temperature is varied and by scanning over a large temperature interval we can directly get information as to which levels are present, what are their concentrations and by using different time/rate windows we can obtain the thermal activation energies of the levels.

There are many ways of constructing a time filter. One of the widely used methods is one in which a variation of the dual-gate boxcar integrator is employed. It precisely determines the emission rate window and provides signal-averaging capabilities to enhance the signal-to-noise ratio, making it possible to defect center having very low concentrations. The use of a double boxcar for rate window selection is illustrated in Figure 2b. The capacitance transients are observed on a fast-response capacitance bridge. A series of transients for a typical defect center are shown on the left-hand side of Fig. 2.8b. These transients are fed into the double boxcar with gates set at t_1 and t_2. The boxcar measures the capacitance at the two times t_1 and t_2. The difference $C(t_1) - C(t_2) = \Delta C$ is calculated. It is clear from the figure that this ΔC goes through a maximum. This ΔC after going through some filtering is converted into the DLTS output S(T) given by (assuming an exponential transient):

$$S(T) = \Delta C_0 \left[\exp(-t_1 / \tau) - \exp(-t_2 / \tau) \right] \tag{14}$$

where ΔC_o is the capacitance change due to the pulse at time t = 0.

It can easily be seen that S(T) really has a maximum for a certain time constant τ_{max}. First consider a transient that is very rapid. Then it has already finished before the first gate opens and hence $C(t_1) = C(t_2)$, and S(T) =0. Similarly when the transient is too slow, it will not change much between the two gates and so again S(T) =0. Thus there will be an output with some maximum value S_{max} only for transients having time constants in between these two.

We can get τ_{max} by differentiating S with respect to t and setting the derivative equal to zero. This gives:

$$\begin{aligned} \tau_{\max} &= (t_1 - t_2 / \ln(t_1 / t_2) \\ &= (x-1)t_1 / \ln(x) \end{aligned} \tag{15}$$

where $x = t_2 / t_1$

Substituting this value in the expression for S gives S_{max} as:

$$S_{\max} = \Delta C_0 \left[\exp(-\ln(x)/(x-1)) - \exp(-x\ln(x)/(x-1)) \right] \tag{16}$$

Thus it is seen that the peak height is independent of the absolute value of t_1 and t_2, rather it depends upon their ratio. Moreover, it is seen that S_{max} is proportional to ΔC_o and therefore to the defect centre concentration N_T. Therefore, the DLTS peak height can directly give the defect centre concentration.

4. Parameters characterizing deep levels by DLTS technique

Below are described some of the ways in which the DLTS technique can be used to study defect centers in semiconductors and to obtain their different characteristic parameters.

4.1. Deep level concentration

As mentioned in the previous section the DLTS signal S is proportional to the magnitude of the capacitance transient ΔC. Equation (12) can be rewritten as

$$\frac{\Delta C}{C_0} = \frac{N_T}{2N_D}$$

where it is assumed that all the traps have been filled.

4.1.1. Transition Distance, λ

The DLTS peak height gives a direct measure of the deep level concentration. Here it must be remarked that in obtaining Eq. (12) the edge region contribution has been neglected. Figure 3 illustrates the edge region in a p-n junction under zero and reverse bias. The distance between the edge of the depletion layer and the point where the Fermi level crosses the trap level is referred to as the transition distance, λ, given by.

http://dx.doi.org/10.5772/59419

$$\lambda = \sqrt{\frac{2\varepsilon\ \varepsilon_0(E_F - E_T)}{q^2 N_D}} \tag{17}$$

where ε_0 and ε are the permittivity of vacuum and of the material, E_f is the Fermi level, E_T is the trap energy level above the valence band, q is the electronic charge and the carrier concentration p is essentially equal to the acceptor concentration, N_a.

In the absence of deep levels and when the doping is uniform, plots of $1/C^2$ vs V are straight lines. However, if the criterion $N_T << N_a$ is not met then the additional capacitance of the charge trapped by deep levels within the distance λ contributes to the measured depletion capacitance. This produces a shoulder in the $1/C^2$ vs V plot at low reverse bias. Also the apparent carrier concentration, $N_{measured}$, as a function of distance, x, deduced from the derivative dC \dV from the same C-V data becomes approximately (for a *uniform* distribution of a single compensating trap level) [13].

$$N_{measured}(x) = N_a(x) - \frac{\lambda}{w} N_T(x) \tag{18}$$

DLTS monitors the capacitance transient associated with the gradual emission of charge from trap centers when the depletion layer is abruptly widened by increasing the applied reverse bias (e. g. switching from V=0 as in Figure. 3a) to V=-V as in Figure 3b)). The calculation of the trap concentration must take into account the fact that the volume within which the charge state of the traps is changed upon the increase of reverse bias and which therefore contributes to the DLTS signal (corresponding to the interval x_2-x_1 in Figure 3) is different to the volume by which the depletion layer is increased (w_2-w_1 in Figure 3).

For exponential transients, this leads to the approximate expression for the trap concentration,

$$N_T = 2\frac{\Delta C}{C} N_a \left(\frac{w_2^2}{x_2^2 - x_1^2} \right) \tag{19}$$

where

$$x_1 = w_1 - \lambda \tag{20}$$

and

$$x_2 = w_2 - \lambda \tag{21}$$

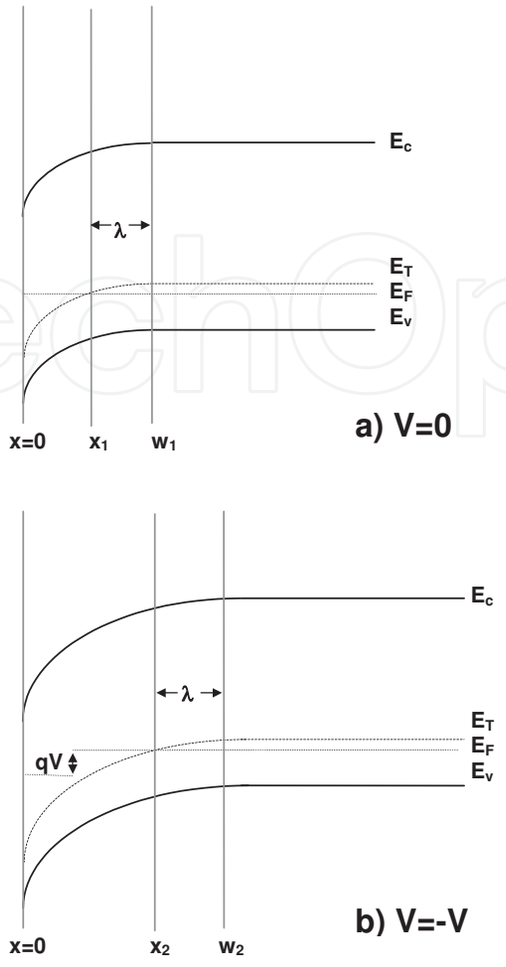

Figure 3. Band diagram of p-type material close to an n+\p junction indicating a deep level at energy E_T above the valence band a) with zero applied bias and b) with applied reverse bias of -V.

The activation energy for emission and the capture cross section of the trap are deduced from an Arrhenius plot of the DLTS maxima as a function of temperature.

As an example of the importance of the inclusion of the transition distance in the calculations, in the case of a sample irradiated with 3 x 10^{16}e /cm^2, p=4 x 10^{14} /cm^3, E_f=0.09 eV at 125K and thus for the di-vacancy with E_T=E_V+0.18 eV, E_f - E_T =0.011 eV. Application of Eq. (17) gives λ=0.48 μm. The Fermi function is of the order of 10^{-3} and to a close approximation the trap is filled with holes. During a fill pulse from -2V to 0V, the depletion region is collapsed from a width of 3 μm at a quiescent bias of -2V to 1.6 μm at zero bias. Thus application of Eqs. (18) to (21) results in an increase of a factor 1.9 in the calculated trap concentration in comparison with the value obtained if the transition distance is ignored.

4.1.2. Non exponential transients

When the condition $N_T << N_a$ is not fulfilled, there is a significant probability that emitted charge will be recaptured before it can be swept out of the depletion region, leading to a non-exponential capacitance transient. In this case, Eq. (19) is no longer appropriate. Several

http://dx.doi.org/10.5772/59419

analyses of this situation exist [1,14] and we have considered the method of Stievenard et al. [13] to calculate a non-exponential transient analysis. In this case, if the transition region is negligibly small then the capacitance transient can be written as

$$\frac{\Delta C}{C} = 1 - \sqrt{1 - \frac{z}{1+z}\exp\left(-et\right)} \tag{22}$$

where $z=N_T/N_a$

4.2. Majority carrier emission rates

The simplest way in which the DLTS technique can be used is the measurement of majority carrier emission. The pulse sequence used is shown in Figure 1b, along with the band diagram and the capacitance transient resulting from such a sequence. The bands have been assumed to be flat for simplicity. The method consists of employing a sufficiently large bias over the sample so as to overcome the edge effects and at the same time be small enough to of lesser value than the break down voltage of the semiconductor. The sample is cooled below the starting measurement temperature. Now bias pulses close to zero volt are repeatedly applied while the sample is reheated. During the pulses, the levels are filled with majority-carriers. As soon as the sample returns to the quiescent reverse bias, the levels start emitting resulting in a transient. During the transient, the capacitance is measured at the pre-set rate window and the DLTS output is plotted as a function of the temperature. Thus we get a peak for each level which has an emission rate within the pre-set time window in the temperature range of scan. The temperature dependence of the emission rate is determined by observing the peak position for several different time windows.

4.3. Minority carrier emission rates

For the observation of minority carrier emission, we have to first fill the level with minority carriers. This is accomplished through minority carrier injection by forward biasing the diode so that a current flows. After the end of the bias pulse, as the sample returns to the quiescent reverse bias, the deep level will emit minority carriers giving rise to a transient. Thus the DLTS measurement is the same as for the majority carrier emission except that the sign of the peak (transient) is now opposite.

4.4. Activation energy

Under thermodynamic equilibrium, the emission rates and the capture coefficients of a deep level are related according to the following equations:

electron emission,

$$e_n = \sigma_n \left\langle v_n \right\rangle_{th} N_C \exp\left(-\frac{E_C - E_T}{kT}\right) \tag{23}$$

where σ_n is the capture cross-section and $\langle v_n \rangle_{th}$ the average thermal velocity of the electron, and N_c is the effective density of states in the conduction band.

hole emission,

$$e_p = \sigma_p \left\langle v_p \right\rangle_{th} N_V \exp\left(-\frac{E_T - E_V}{kT} \right) \tag{24}$$

where σ_p is the capture cross-section and $\langle v_p \rangle_{th}$ the average thermal velocity of the hole, and N_V is the effective density of states in the valence band.

Thus the emission rate variation with temperature is given by

$$e_{n,p} \propto \exp(-1/T) \tag{25}$$

Hence a plot of log(e) versus $1/T_{pk}$, where T_{pk} is the temperature position of the peak in the corresponding time window, gives a straight line with the slope $-E_A/kT$, where E_A is the activation energy of the level. Such a plot is known as an Arrhenius Plot. From the intersection of the plotted line with 1/T = 0, the capture cross-section $\sigma_{n,p}$ at T = ∞ can be calculated.

One may often encounter plots of $\log(e/T^2)$ versus 1/T instead of log(e) versus 1/T. The factor T^2 comes in because of the temperature dependence of $\langle v_{th} \rangle$ and effective density of states $N_{C,V}$. The activation energy thus obtained may still not be the true activation energy because in some cases, the capture cross-section is found to be temperature dependent. Thus the true thermal activation energy in such cases would be obtainable if the temperature dependence of capture cross-section is first determined independently and then the relevant correction is applied to the apparent activation energy.

4.5. Measurement of capture cross-section

The third important parameter for identifying a defect centre is the capture cross-section $\sigma_{n,p}$. One can extrapolate the Arrhenius plot to 1/T = 0 and obtain the capture cross-section at T = ∞ from the intercept. But this usually leads to a far from true value of the capture cross-section because of the following two reasons: a) $\sigma_{n,p}$ may be temperature dependent and hence the extrapolation is not valid; b) a slight error in extrapolation may lead to several orders of magnitude difference in values of capture cross-section. Hence, the capture cross-section must be directly measured whenever possible and over as long a range of temperatures as possible.

Measurement of majority carrier capture cross-section is relatively simple as compared to minority carrier capture cross-section measurements. A fixed emission rate is chosen and DLTS scans carried out while the filling pulse-width is varied from scan to scan. As the pulse width increases from a small value so does the peak height until for a certain value of pulse width, it reaches a maximum i.e. at this value all defect centers are completely filled during a single

http://dx.doi.org/10.5772/59419

saturation pulse. The peak height is related to the filling pulse width t_p via the following equation:

$$1-S/S_{\infty} = \exp(-t_p / \tau) \tag{26}$$

where S is the peak height for any pulse width t_p and S_∞ the saturated peak height.

The slope of $\ln(1-S/S_\infty)$ versus t_p gives $1/\tau$.

now

$$\sigma_n = 1/(\tau n \langle V_{th} \rangle) \tag{27}$$

Thus capture cross-section is known if n and $<v_{th}>$ are known.

The calculation of capture cross-sections for minority carriers is complicated due to the difficulty in determining the concentration of electrons/holes, which is a function of the current during the injection pulse.

5. Application of DLTS technique on photovoltaic materials

5.1. Radiation-induced recombination centers in Si

In order to clarify the origins of radiation-induced defects in Si and correlation between their behavior and Si solar cell properties, DLTS analysis has been carried out. DLTS measurements were made using a quiescent bias of -2V and a saturating fill pulse of 2V, 1 ms duration. Figure. 4 shows both the majority- and minority-carrier DLTS spectra of some of the same Si diode as a function of 1 MeV electron fluence. A large concentration of a minority carrier trap with an activation energy of about E_C-0.18 eV has been observed, as well as the majority carrier traps at around E_v+0.18eV and E_v+0.36eV.

A comparison of the total majority carrier defect concentration observed by DLTS with the measured change in carrier concentration for all the diodes is made in Figure 5. The compensation observed in the C-V profile is mainly caused by the minority carrier trap E_C-0.18 eV shown in Figure 4. The total concentrations of these majority-carrier traps and the minority-carrier trap at around E_c-0.18eV have been found to be nearly equal to the change in carrier concentrations. The concentration of the minority carrier trap at around E_c-0.18eV, was high enough to be responsible for most of the observed compensation and subsequently type conversion of the base layer from p to n-type. The E_v+0.36eV defect is thought to be responsible for minority-carrier lifetime (diffusion length) deg radiation according to the annealing experiments in the higher temperature range as will be described below. This means that the E_v+0.36eV is thought to act as a recombination center, in addition to a role as a majority-carrier trap center.

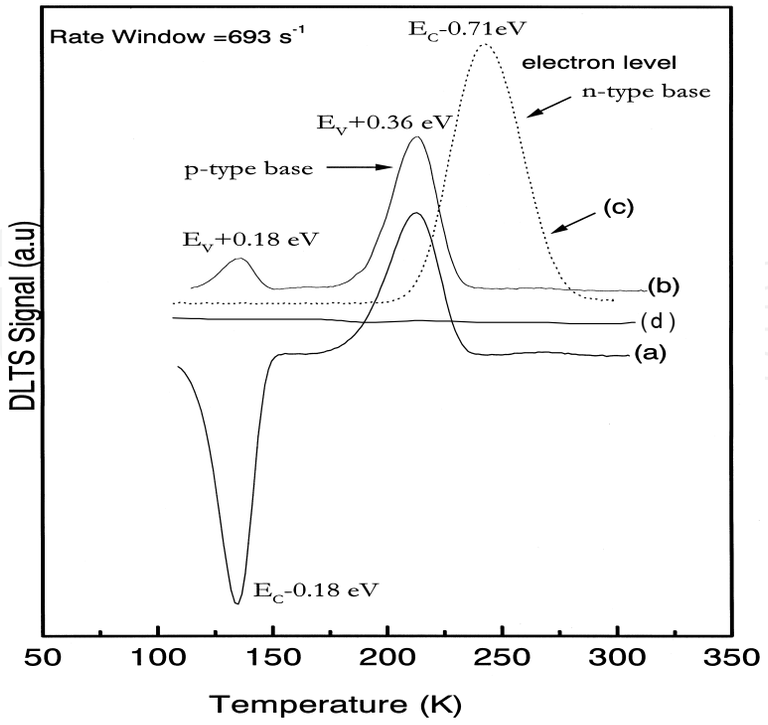

Figure 4. DLTS spectra of p-type Si before and after 1 MeV electron irradiation: (d) before irradiation, (b) and (a) majority and minority carrier signals after 1 x 10^{16} cm^{-2} fluence, respectively and (c) majority carrier signal after 1 x 10^{17} cm^{-2} fluence. The base of the diode irradiated with 1 x 10^{17} cm^{-2} electrons was n-type and required a correction to the spectrum to account for the effects of series resistance.

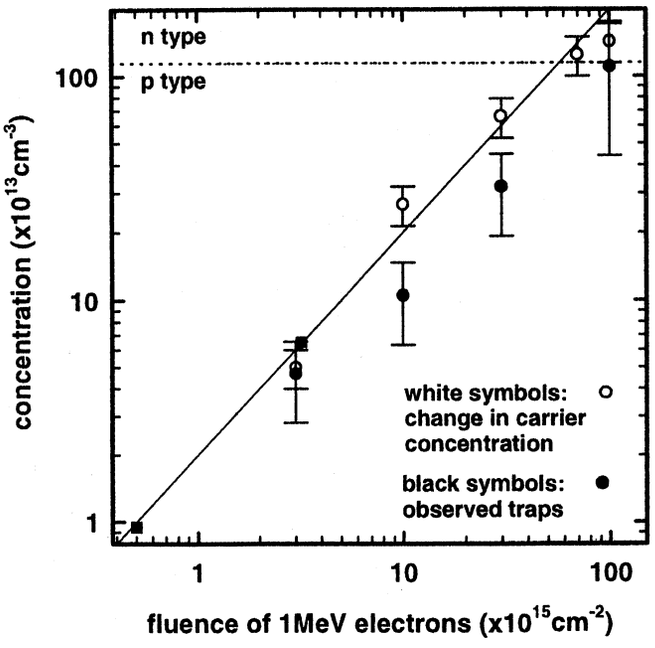

Figure 5. Total trap concentration observed by DLTS in comparison with the change in carrier concentration observed by C-V measurements at 300 K as a function of 1 MeV electron fluence.[15]

http://dx.doi.org/10.5772/59419

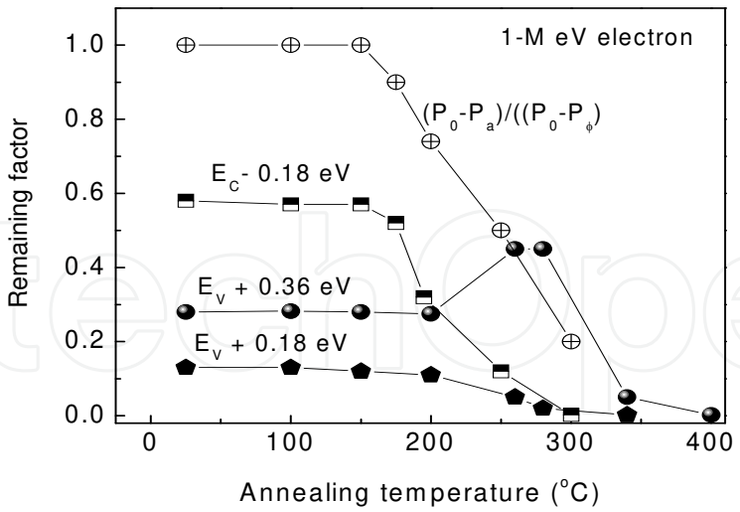

Figure 6. Comparison of isochronal annealing of densities of E_c-0.18eV, E_v+0.18eV and E_v+0.36eV defect centers measured by DLTS with that of carrier concentration of p-type Si irradiated with 1-MeV electrons. Each annealing step duration was 20 min.[15].

It is important to note that after annealing at 250°C, although the carrier concentration had recovered substantially, the observed concentration of the E_v+0.36eV defects had increased as shown in the Figure 6. This suggests that the E_v+0.36eV defects are not principally responsible for carrier removal.

We were able to confirm that the degradation of lifetime (diffusion length) is likely to be caused by the introduction of dominant hole level E_v+0.36eV and annealing behavior of this level govern the diffusion length recovery [15]. Figure 7 compares isochronal annealing of density of the majority-carrier trap at E_v+0.36eV measured by DLTS and that of recombination center determined by solar cell properties in p-type Si irradiated with 1-MeV electrons. Changes in the relative recombination center density N_r with annealing were also estimated by changes in short-circuit current density J_{sc} of the solar cell according to the following equation:

$$\frac{N_{ra}}{N_{r\varphi}} = \frac{\Delta(1/L_a^2)}{\Delta(1/L_\varphi^2)} = \frac{\left[1/L_a^2 - 1/L_0^2\right]}{\left[1/L_\varphi^2 - 1/L_0^2\right]} \sim \frac{\Delta(1/J_{sca}^2)}{\Delta(1/J_{sc\varphi}^2)} = \frac{\left[1/J_{sca}^2 - 1/J_{sco}^2\right]}{\left[1/J_{sc\varphi}^2 - 1/J_{sco}^2\right]} \tag{28}$$

Features of the E_v+0.36eV majority-carrier trap center with reverse annealing stage at 200^0 C~300^0 C and a recovery stage at around 350^0 C are similar to the changes in minority-carrier diffusion length L determined from the solar cell properties. This implies that the E_v+0.36eV majority-carrier trap center may also act as a recombination center.

As shown in Figure 6 the estimated initial concentration of the trap at approximately E_C-0.18eV is about 60% of the change in carrier concentration and therefore populous enough to be the dominating influence. Furthermore, the recovery of the carrier concentration after annealing occurs over roughly the same temperature range as disappearance of the minority trap signal.

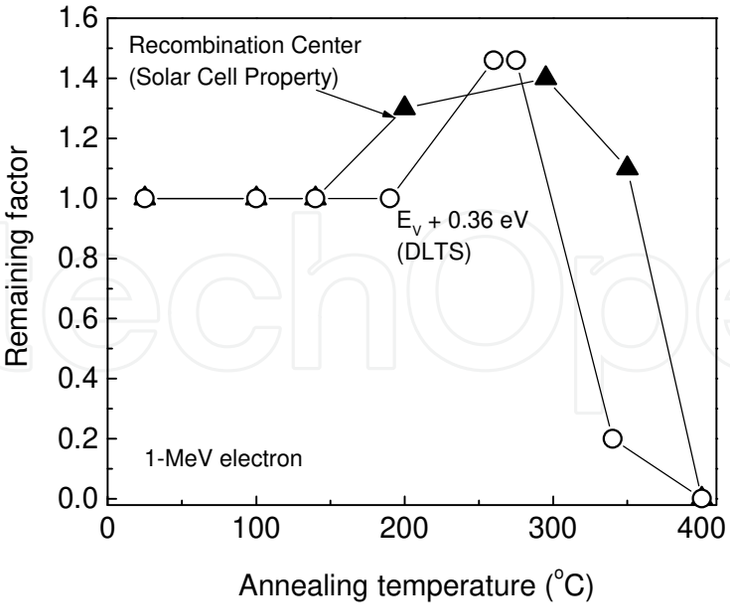

Figure 7. Comparison of isochronal annealing of the majority-carrier trap at E_v+0.36eV measured by DLTS with that of the dominant recombination center determined by solar cell properties in p-type Si irradiated with 1-MeV electrons [15].

This evidence is, therefore, coherent with the hypothesis that the E_c-0.18 eV center is mainly responsible for the compensation of the base layer. The radiation-induced traps, which play an important role regarding the carrier removal and conduction type conversion of the base region, should be principally deep-level donors, which must be positively charged before electron capture.

$$X^+ + e^- \leftrightarrow X^0 \tag{29}$$

5.2. Role of boron on compensator center

Interestingly, the introduction rate of the E_C-0.18eV electron level in B-doped samples is strongly boron concentration dependent. Comparison of introduction behavior, annealing kinetics and the strong relation to boron and oxygen contents, supports correlation of this level (E_C-0.18eV) with the B_i-O_i (Figure 8).

5.3. Role of gallium on compensator center

One of the most interesting and technological important feature of our work was the disappearance of the dominant donor like electron level E_C-0.18 eV in Ga-doped CZ- grown samples [17] (Figure 9). As we have discussed above this level acts as a compensator center, which is positive charge before electron capture. The concentration of this level is about 60% of the change in carrier concentration after heavy fluences and therefore populous enough to be the dominating influence on device performance. This implies that carrier removal effects can be

http://dx.doi.org/10.5772/59419

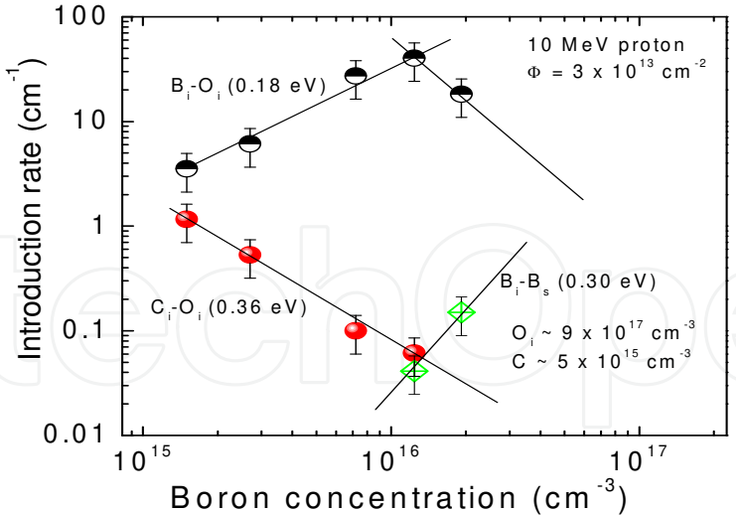

Figure 8. Introduction rates of the interstitial related defects in 10 MeV proton irradiated p-Si as a function of background impurity concentration [16].

partially offset by using Ga as dopant instead of boron. The absence of this level in Ga-doped Si gives support that this center in B-doped Si is related to B_i-O_i [18-20] complex.

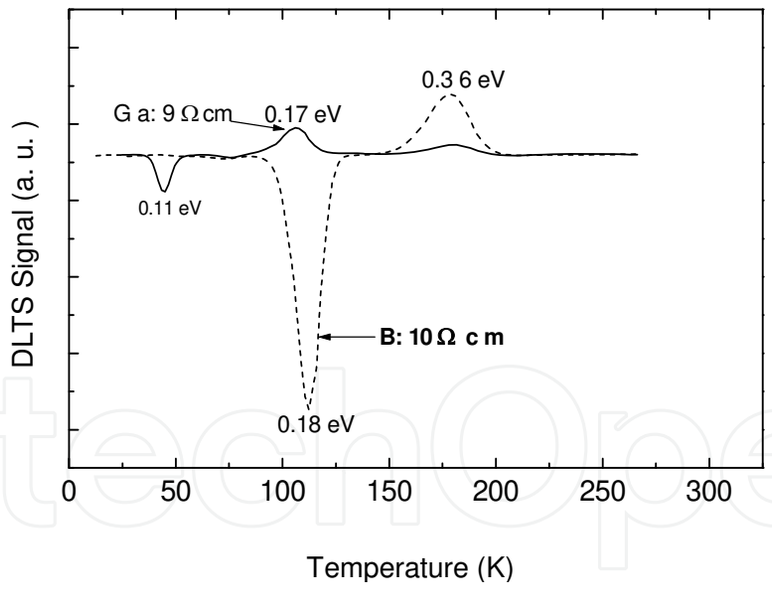

Figure 9. Comparison of the minority carrier DLTS spectra measured for boron-or gallium –doped CZ-grown Si irradiated with 1-MeV 3 x 10^{16} electrons/cm^2. The spectra were acquired using a reverse bias of 2 V, a pulse voltage of -1.5V, a pulse width of 1x 10^{-3} s and period width of 200 ms. [17].

5.4. Superior radiation resistance of InGaP solar cells

In this section, we present the direct observation of minority-carrier injection annealing of the dominant 1 MeV electron irradiation-induced hole trap labeled H2 located at 0.50-0.55 eV

above the valence band in p-InGaP by Deep Level Transient Spectroscopy (DLTS). Furthermore, an evidence of a large minority carrier capture cross section for this hole trap has been obtained by double-carrier pulse DLTS which demonstrate the important role of this trap as an recombination center. The one aim of present study was to clarify the mechanism involved in minority-carrier injection-enhanced annealing of the radiation-induced defect H2 in p-InGaP [22-27].

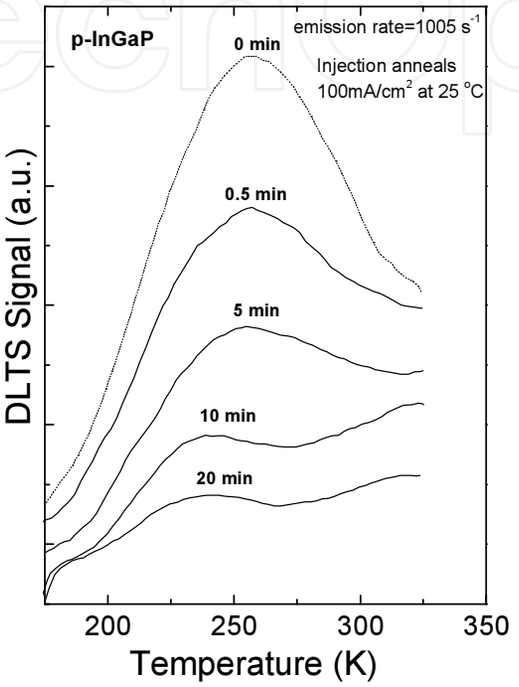

Figure 10. Changes of the DLTS spectrum of trap H2 with various time of injection at 25°C with an injection density of 0.1 A cm^{-2} [21].

The important result of this study is the influence of minority-carrier injection on the annealing kinetics of dominant hole level H2 [21]. In order to clarify the recovery of the solar cells properties following minority-carrier injection annealing, we carried out a systematic study of the variation of the concentration of the hole level H2 using a constant amplitude of forward bias injection (0.1 A/cm^2) at various temperatures for 0.5, 1, 2, 5, 10 and 20 min. The majority-carrier emission DLTS scans taken after different forward bias injection steps show a pronounced reduction in the H2 amplitude as shown in Figure. 10, which is correlated with a recovery of the maximum power output of the solar cells. It should be noted that the H2 peak; is rather broad and after pronounced reduction following forward bias, exhibits a double structure, indicating that this peak consists of more than one closely spaced peaks; one on the high temperature side appear to anneal relatively slowly

Figure 11 presents the temperature dependence of the annealing rate A^* of the hole trap H2 by minority-carrier injection-enhanced processes, determined from DLTS.

A comparison is given with the injection-enhanced annealing rates estimated by changes in short-circuit current density J_{sc} of the solar cells according to the following:

http://dx.doi.org/10.5772/59419

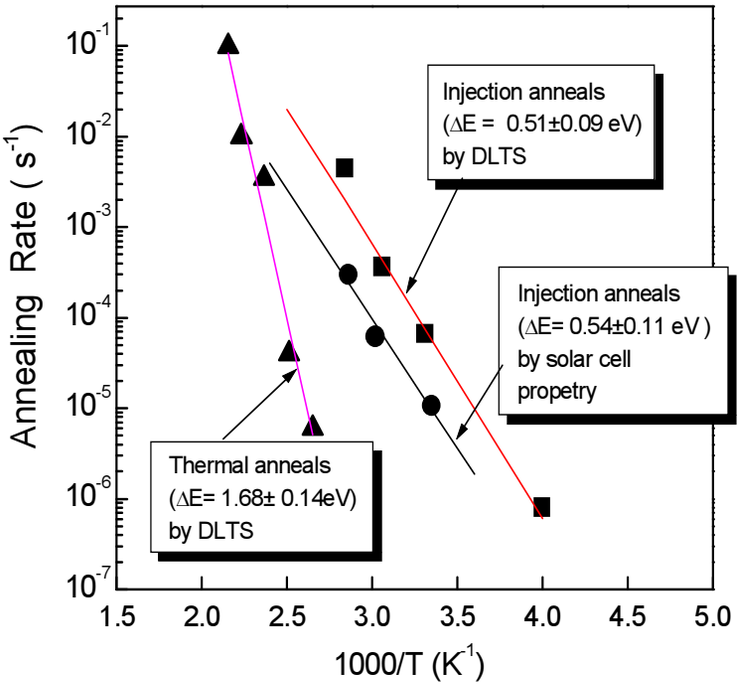

Figure 11. Temperature dependence of the thermal and injection annealing rates of the radiation-induced defects in p-InGaP, determined from solar cells property (J_{sc} or L) and for H2 trap observed by DLTS [21].

$$\frac{N_{TI}}{N_{T\varphi}} = \frac{L_{\varphi}^2(L_0^2 - L_I^2)}{\left[L_I^2(L_0^2 - L_{\varphi}^2)\right]} \sim \frac{J_{sc\varphi}^2(J_{sc0}^2 - J_{scI}^2)}{\left[J_{scI}^2(J_{sa0}^2 - J_{sc\varphi}^2)\right]} \tag{30}$$

where suffixes 0, φ, and I correspond to before and after irradiation, and after injection, respectively. The important result of this study is the direct relationship between the annealing rates, the solar cells properties and the H2 trap.

A close agreement between activation energy for recovery of radiation-induced defects, determined by solar cell properties and for the hole traps H2, demonstrates that this trap controls the minority-carrier lifetime. This result demonstrates that the dominant majority hole level H2 (E_V+0.5–0.55 eV) is the recombination center, which governs the minority-carrier lifetime in n^+–p InGaP solar cells.

5.5. Superior radiation resistance of AlInGaP solar cells

Figure 12 presents the temperature dependence of the annealing rate A of the trap H1, in p-AlInGaP determined by DLTS. The annealing activation energy of electron irradiation-induced defect H1 in p-AlInGaP is evaluated to be 0.50eV. A comparison is provided with the injection-enhanced annealing rates estimated for the defect H2 in p-InGaP. It is to be noted that the minority carrier injection annealing properties of the defect H2 in p-InGaP observed in the previous 1 MeV electron study are almost the same as those observed in the present study of H1 defect in p-AlInGaP after 1 MeV electron irradiation, which identified that the defect H1

observed in p-AlInGaP has the same nature of the defect H2 previously observed in P-InGaP and H4 in InP [28,29].

The recovery of the radiation damage due to minority carrier injection under forward bias is thought to be caused by an energy release mechanism in which enhancement is induced by the energy released when a minority carrier is trapped on the defect site. According to this mechanism, a change of charge states due to capture of carriers can result in electron phonon coupling. That is, vibration relaxation occurs, which may activate various reactions of the defect such as its migration or destruction, and ultimately decays to heat the lattice. The detailed analysis of this mechanism was previously studied in case of defects in InP, GaAs, and InGaP by the authors and others.

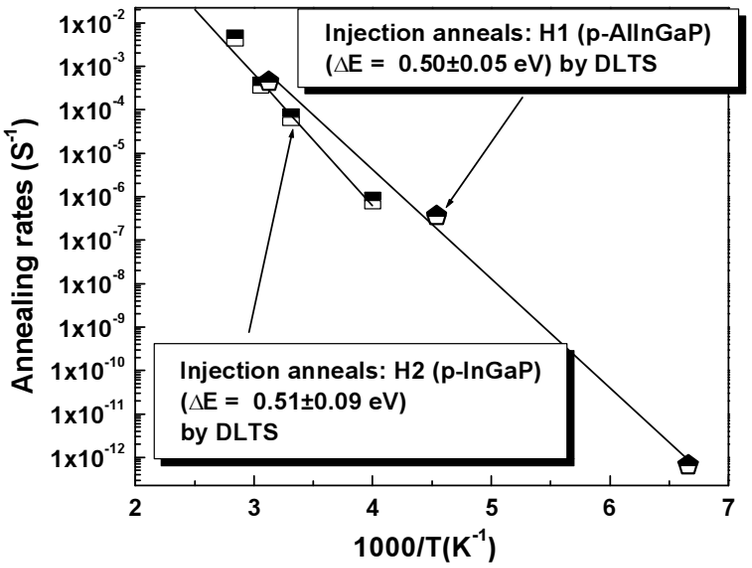

Figure 12. Comparison of the temperature dependence of injection annealing rates of the radiation-induced defect H1 (E_V+0.37eV) in p-AlInGaP and H2 (E_V+0.55eV) in p-InGaP [29].

5.6. Self-annihilation of electron irradiation induced defects in $InAs_XP_{1-X}$/InP multiquantum well solar cells

In this study, the authors demonstrated the direct observation of majority and minority carrier defects in $InAs_xP_{1-x}$/InP diodes and solar cells structures before, and after 1MeV electron irradiation by double-correlation deep level transient spectroscopy (DDLTS) in order to further evaluate the potential use of this material for space applications [30].

In order to electrically characterize radiation-induced deep center in InAsxP1-x/InP quantum well structure, the DDLTS technique is used to explore the recombination characteristics of deep levels in $InAs_xP_{1-x}$/InP multiquantum well solar cell structures.

The activation energy and apparent capture cross sections are determined to be 0.65 eV and 4.3 x 10^{-14} cm^2. The apparent high capture cross section of E1, suggests that this level might act as a strong recombination center.

http://dx.doi.org/10.5772/59419

We observed an unexpected and interesting reduction in the strength of the peak E1 in our deep level spectrum recorded subsequent to a room temperature storage of the irradiated device. Consequently, we carried out a detailed study of the room temperature isothermal annealing effects and carefully monitored the various deep-level peaks in our spectra as a function of sample storage time at room temperature (25°C). The dashed DLTS curve of Figure 13 represents a spectrum recorded after 90 days storage at room temperature and the significant reduction in the intensity of the E1 peak.

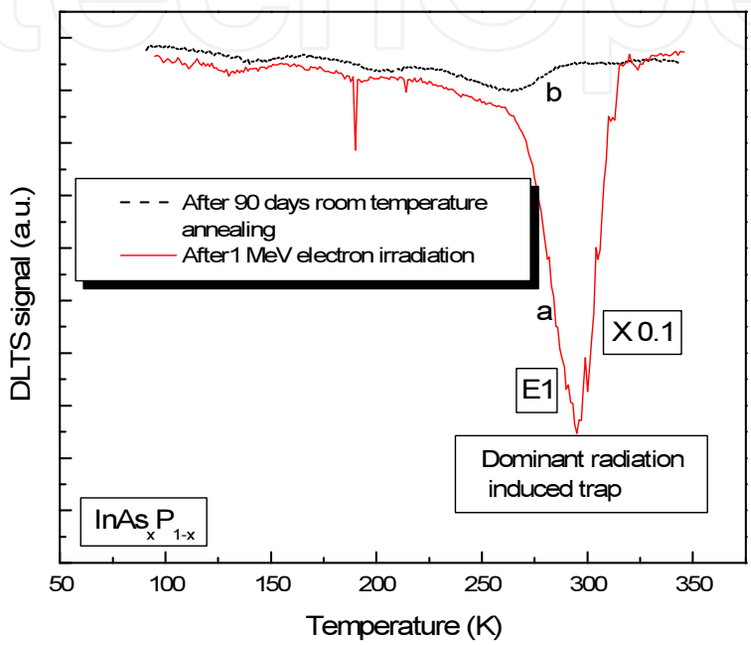

Figure 13. Room temperature annealing effects: (a) after irradiation (b) after 90 days storage at room temperature following irradiation [30].

The activation energy and apparent capture cross sections are determined to be 0.65eV and 4.3 x 10^{-14} cm^2. The apparent capture cross section of E1 is very high, which indicates that it may act as a strong recombination center. However, serendipitously long duration room temperature storage of the device yielded a total annihilation of E1. Although the detailed mechanisms at play are not fully understood, the serendipitous findings reported here clearly demonstrate the fact that insertion of QWs in the intrinsic region of an InP p-i-n solar cell results in a more radiation tolerant devices.

6. Summary

DLTS is an effective spectroscopy technique for processing transient (capacitance or current) from deep levels. This technique has proved to be an instrumental in determining most of the properties of the defects such as structure, introduction rates, introduction mechanism, thermal stability of the defects etc. DLTS is particularly attractive because it can be used to

characterize defects using various kinds of space charge based devices such as Schottky barrier diodes, and p-n junction to quantum well based complex devices. In addition, sensitivity of the DLTS for detecting defects in concentration of 10^9 cm^{-3} is superior to any other characterization technique. In this chapter we have reviewed the extensive work done by the authors, on the electronic properties of the recombination and compensator centers in Si and III-V compound materials for space and terrestrial solar cells.

Deep level transient spectroscopy (DLTS) is the best technique for monitoring and characterizing deep levels introduced intentionally or occurring naturally in semiconductor materials and complete devices. DLTS has the advantage over all the techniques used to-date in that it fulfils almost all the requirements for a complete characterization of a deep center and their correlation with the device properties. In particular the method can determine the activation energy of a deep level, its capture cross-section and concentration and can distinguish between traps and recombination centers.

In this chapter we provide an overview of the extensive R & D work that has been carried out by the authors on the identification of the recombination and compensator centers in Si and III-V compound materials for space solar cells. In addition, we present an overview of key problems that remain in the understanding of the role of the point defects and their correlation with the solar cell parameters.

Author details

Aurangzeb Khan[1*] and Yamaguchi Masafumi[2]

*Address all correspondence to: akhan@southalabama.edu

1 Department of Electrical and Computer Engineering, University of South Alabama, Mobile, AL, USA

2 Toyota Technological Institute, 2-12-1 Hisakata, Tempaku, Nagoya, Japan

This chapter is an expanded version of the authors' earlier proceedings paper [31] (© 2006 IEEE. Excerpts reprined with permission).

References

[1] D. V. Lang, J. Appl. Phys. 45, 3023 (1974).

[2] C. T. Sah and J. W. Walker, Appl. Phys. Lett. 22, 384 (1973).

[3] J. C. Carballes, J. Varon and T. Ceva, Solid State Commun. 9, 1627 (1971).

[4] D. L. Losee, Appl. Phys. Lett. 21, 54 (1972).

[5] R. Williams, J. Appl. Phys. 37, 3411 (1966).

[6] C. T. Sah L. Forbes, L. L. Rosier, and A. F. Tasch Jr., Solid State Electron. 13, 759 (1970).

[7] L. D. Yau and C. T. Sah, Phys. Status Solidi A 6, 561 (1971).

[8] C. H. Henry H. Kukimoto, G. L. Miller and F. R. Merritt, Phys. Rev. B 7, 2499 (1973).

[9] H. Kukimoto, C. H. Henry and F. R. Merritt, Phys. Rev. B 7, 2486 (1973).

[10] D. V. Lang, *Topics in Applied Physics - Thermally Stimulated Relaxation in Solids*, Vol. 37, ed. P. Bräunlich, Soringer Verlag, New York, (1979).

[11] W. Shockley and W. T. Read Jr., Phys. Rev. 87, 835 (1952).

[12] R. N. Hall, Phys. Rev. 83, 228 (1951).

[13] D. Stievenard, M. Lannoo and J. C. Bourgoin, Solid State Electronics 28, 485 (1985).

[14] L. C. Kimerling, J. Appl. Phys. 45, 1839 (1974).

[15] M. Yamaguchi, A. Khan, S. J. Taylor, K. Ando, T. Yamaguchi, S. Matsuda, and T. Aburaya, J. Appl. Phys. 86, 217 (1999).

[16] A. Khan, M. Yamaguchi, M. Kaneiwa, T. Saga T. Abe, O. Annzawa and S. Matsuda. J. Appl. Phys. 90, 1170(2001).

[17] A. Khan, M. Yamaguchi, M. Kaneiwa, T. Saga T. Abe, O. Annzawa and S. Matsuda. J. Appl. Phys. 87, 8389 (2000).

[18] A. Khan, M. Yamaguchi, S. J. Taylor, T. Hisamatsu and S. Matsuda, Jpn. J. Appl. Phys. 1, 38, 2679, (1999).

[19] A. Khan, M. Yamaguchi, T. Hisamatsu and S. Matsuda, J. Appl. Phys. 87, 2162 (2000).

[20] P. M. Mooney, L.J. Cheng, M. Sull, J. D. Gerson, and J. W. Corbett, Phy. Rev. B 15, 3836 (1977).

[21] A. Khan, M. Yamaguchi, J.C. Bourgoin and T. Takamoto., Appl. Phys. Lett. 76, 2550 (2000).

[22] J. C. Bourgoin and J. W. Corbett, Radiation Effects 36, 157 (1978).

[23] L. C. Kimerling, Solid State Electronics, 21, 1391 (1978).

[24] L. C. Kimerling and D. V. Lang, Inst. Phys.Conf. Ser. 23, 589 (1975).

[25] J. C. Bourgoin and J. W. Corbett, Phys. Lett. 83A, 135 (1972).

[26] J. C. Bourgoin and J. W. Corbett, Inst. Phys. Conf. Ser. 23, 149 (1975).

[27] D. V. Lang and L. C. Kimerling, Phys. Rev. Lett. 35, 22 (1975).

[28] A. Khan, Masafumi Yamaguchi, Jacques C. Bourgoin, and Tatsuya Takamoto. J. Appl. Phys. 89, 4263 (2001).

[29] A. Khan, S. Marupaduga, M. Alam, N. J. Ekins-Daukes, Appl. Phys. Lett. 85, 5218 (2004).

[30] A. Khan, A. Freundlich J. Gou, A. Gapud, M. Imazumi, and M.Yamaguchi, "Self-annihilation of electron-irradiation-induced defects in $InAs_XP_{1-X}$/InP multiquantum-well solar cells," *Applied Physics Letters*, vol. 90, p. 233111, 2007.

[31] A. Khan, Masafumi Yamaguchi, Hae-Seok Lee, Nicholas J. Ekins-Daukes, Tatsuya Takamoto, Mitsuru Imaizumi, Steve Taylor, in Proc. of 4th World Conference and Exhibition on Photovoltaic Solar energy Conversion (WCPEC-4), Hilton Waikoloa Village, Waikoloa, Hawaii, May 7-12, 2006, p. 1763.